KFUPM
Journal of Undergraduate Research International

Diamond Open Access 14

Article Chemistry/Material Science and Engineering

Nitrogen-Doped Carbon Dots from Pomegranate Peels as Sustainable Corrosion Inhibitors for Carbon Steel in Acidic Medium

Ali M. Al Nasser, Hifsa Kurdshid, and Saviour A. Umoren*

Cite https://doi.org/10.64589/juri/214906

Submitted: July 28, 2025 **Revised:** October 29, 2025 **Accepted:** November 30, 2025

ABSTRACT

Carbon steel suffers from rapid corrosion in acidic environments such as those encountered during acid cleaning and petroleum-well acidification, leading to significant economic losses and environmental challenges. Conventional corrosion inhibitors are often toxic, nonbiodegradable, and expensive, motivating the search for sustainable biomass-derived alternatives. In this study, carbon dots (CDs) synthesized from pomegranate peel waste (PPCDs) and their nitrogen-doped analogs (N-PPCDs) were evaluated as ecofriendly corrosion inhibitors for carbon steel in 5 wt.% HCl. The structural, morphological, and chemical properties of the materials were characterized using UV-Vis, Fourier-transform infrared, transmission electron microscopy, and energy-dispersive X-ray analyses. Electrochemical impedance spectroscopy and potentiodynamic polarization measurements demonstrated that both PPCDs and N-PPCDs acted as mixed-type inhibitors, effectively inhibiting both anodic and cathodic corrosion reactions. Nitrogen doping enhanced inhibition efficiency from 70% to 80% at CD concentration of 200 ppm owing to enhanced adsorption and chemisorption through N- and O-donor functional groups, as confirmed by surface analysis. These findings establish the nitrogen-doped pomegranate peel CDs as promising and sustainable alternatives to conventional synthetic inhibitors for corrosion control in acidic media.

Keywords: carbon dots, pomegranate peel, carbon steel, acid corrosion, corrosion inhibition

1. INTRODUCTION

Corrosion has been a significant and long-standing challenge, as it affects a wide spectrum of sectors, such as transportation, construction, and energy sectors, leading to structural failures, operational inefficiencies, and high maintenance costs [1]. Carbon steel (CS), despite its widespread use, is particularly vulnerable to corrosion in acidic environments, for example, when exposed to acidic cleaning agents or harsh environments [2], necessitating the development of effective corrosion inhibitors. While many corrosion inhibitors have been shown to be effective, they are often toxic and expensive [3]. This has intensified research into greener alternatives capable of offering comparable or superior inhibition performance while minimizing ecological impact [4]. Hence, there is a demand for robust and environmentally friendly corrosion inhibitors that can perform in extreme environments. In meeting this demand, green corrosion inhibitors offer several advantages, such as a lack of toxicity and the utilization of inexpensive waste resources [5]. Recently, carbon dots (CDs) synthesized from agricultural waste have attracted significant attention [6]. These CDs are nanosized and may be derived from a variety of low-cost materials, such as carbohydrates and organic solvents [7]. CDs synthesized from renewable biomass and agricultural waste precursors, such as fruits, vegetables, and dairy byproducts, offer advantages over traditional inhibitors, because these precursors are non-toxic, cost-effective, and environmentally friendly [8]. Reports have shown that CDs can effectively suppress corrosion in acidic media by blocking metal's active sites, hindering electron transfer, and establishing barrier films that restrict the ingress of aggressive species [9]. In addition, CDs can serve as electron donors and acceptors, enhancing its corrosion-inhibition properties [10]. Incorporation of nitrogen into CDs, in particular, has been found to enhance their inhibition capability due to improved electron-donor characteristics and stronger metal–inhibitor interactions [4], improving their ability to donate electrons, suppress electrochemical reactions, and provide corrosion protection. Several studies have demonstrated that N-doped CDs can reduce the corrosion rate of CS in hydrochloric acid, with the nitrogenated functional groups strengthening the adsorption process [11]. For instance, carbon-dot-based complexes modified with sulfosalicylic acid served as corrosion inhibitors for CS in an HCl solution, markedly decreasing the corrosion rate [12]. Biomass-derived CDs were employed as corrosion inhibitors for Q235 steel in a 1 M HCl solution, mitigating corrosion by self-aggregation and adsorption onto the metal surface [13]. Additionally, the efficacy of CDs as corrosion inhibitors for CS has been evidenced in various acidic solutions, with the diminished corrosion rate ascribed to the development of a protective coating on the metal surface [14–16]. While CDs derived from various natural and synthetic sources have demonstrated considerable potential

as corrosion inhibitors for various metals under diverse environmental conditions[4,8], the use of CDs derived from pomegranate peels for corrosion protection of CS has not been reported to date. Furthermore, nitrogen-doped CDs are an emerging class of functional nanomaterials that have received limited attention in the context of corrosion inhibition. This study addresses this gap by investigating CDs synthesized from pomegranate peel waste (PPCDs) and their nitrogen-doped analogs (N-PPCDs) obtained via hydrothermal carbonization of pomegranate peel waste using glycine for N doping. The inhibition of CS in HCl was evaluated through electrochemical and surface analyses, highlighting their potential as sustainable high-performance corrosion inhibitors.

2. EXPERIMENTAL

2.1. Materials and Materials Preparation. Pomegranates were purchased from a local market and glycine was obtained from Sigma-Aldrich. X60 CS was used as the metal substrate, and its chemical composition matched that previously documented in the literature[17]. The corrosive medium used in the research work was 5% solution of hydrochloric acid (HCl). It was prepared by diluting analytical-grade concentrated HCl (Merck) with distilled water. The CS samples were polished by wet mechanical abrasion using sandpapers of different grades (#120, #320, #600, #800, and #1000). Prior to each experimental run, the polished samples were thoroughly rinsed with distilled water, followed by ethanol, and subsequently dried using warm air to ensure a clean, uniform surface.

2.2. Synthesis of Undoped and N-doped PPCDs. The pomegranate peel waste was sun-dried, and the dried biomass was ground into a fine powder that served as the carbon source. Glycine was used as the nitrogen source. The pomegranate peel (1.5 g) and glycine (0.5 g) precursors were mixed with distilled water (100 mL) and placed in a Teflon-lined stainless-steel autoclave. To facilitate the hydrothermal process, the autoclave was kept in a drying oven at 200 °C for a full day. Once the reaction finished, the autoclave was cooled to room temperature, and the mixture was filtered using Whatman #1 filter paper. To purify the CDs, the supernatant was filtered. The dialyzed filtrate was then dried in an oven (70 °)C to produce the solid-state product (N-PPCDs). A solid product obtained from the powdered pomegranate peel waste material without blending with glycine is referred to as the undoped pomegranate peel CDs (PPCDs).

2.3. Characterization of Synthesized PPCDs. The optical properties of PPCDs and N-PPCDs were examined using a JASCO 770 UV–vis spectrophotometer (Tokyo, Japan) operated at a scanning speed of 200 nm min^{-1} and a spectral resolution of 1 nm. Distilled water served as the reference for baseline correction. Fourier-transform infrared (FTIR) spectra were collected with an ATR-FTIR system (Nicolet iS5, Thermo Scientific, Waltham, MA, USA) over the wavenumber range of 4000–400 cm^{-1}. Morphological observations were performed using a JEOL JSM-6610LV scanning electron microscope (JEOL, Japan). For SEM analysis, a drop of the ethanolic dispersion of PPCDs or N-PPCDs was deposited onto an aluminum stub, allowed to dry at ambient conditions to form a thin film, and subsequently coated with a thin layer of gold. Imaging was conducted at an accelerating voltage of 20 kV. Elemental composition was evaluated using an energy-dispersive X-ray spectroscopy (EDAX) detector integrated with the SEM system. Transmission electron microscopy (TEM) was used to determine particle size and morphology. Samples were prepared by placing a small amount of the colloidal PPCD or N-PPCD suspension onto a carbon-coated copper grid, followed by drying at room temperature. TEM images were obtained using a JEOL JEM-2100F microscope (Tokyo, Japan) operated at 200 kV[15].

2.4. Corrosion Inhibition Evaluation. The inhibitory effectiveness of PPCDs and N-PPCDs on CS in 5 wt.% HCl was evaluated using weight loss and electrochemical measurements. The equations (1 and 2) and a detail description of the experimental procedures used for weight loss evaluation are provided in Section S5 and Table S2 of the Supplementary Materials. A Gamry 1010E system was employed to conduct the electrochemical tests in accordance with the protocol detailed in Section S6. Linear polarization resistance (LPR) quantities were estimated by scanning ±10 mV around the corrosion potential (E_{corr}) at a rate of 0.167 mV/s, whereas potentiodynamic polarization (PDP) measurements were conducted over a range of ±250 mV using a scan rate of 0.5 mV/s. Data analysis was conducted by Echem Analyst v6.2 software. The inhibition efficiencies (IE) were calculated using Equations (3) and (4) in Table S2, corresponding to the PDP, EIS, and LPR methods.

2.5. Surface Analysis. The surface morphology of the carbon steel samples was examined using a scanning electron microscope (SEM; JEOL JSM-6610LV, Japan) equipped with an energy-dispersive X-ray spectroscopy (EDAX) system. This combination enabled both imaging and elemental analysis of the sample surfaces after exposure to the corrosive environment, with and without the presence of inhibitors. The method for the preparation of the sample for SEM analysis is described in Section S7 of the Supplementary Materials. In addition, a 3D optical profiler (Profilm 3D, Filmetrics, USA) was used to evaluate alterations in the surface topography of the steel specimens. This analysis was performed on samples exposed to 5% HCl under inhibited and uninhibited conditions to assess changes in roughness and damage features. AFM measurements were conducted using an MFP-3D Infinity Oxford Instruments (UK), operated under ambient conditions, to provide nanoscale insight into surface modifications resulting from corrosion and inhibitor adsorption.

3. RESULTS AND DISCUSSION

3.1. Characterization of PPCDs and N-PPCDs. Prior to the examination of the corrosion inhibition by the CDs, characterization techniques were used to verify the successful synthesis of PPCDs and N-PPCDs. TEM analysis (Figure 1a) revealed that PPCDs exhibit an amorphous spherical morphology, with particle sizes ranging from 5 to 10 nm. The UV–vis spectrum (Figure 1b) of PPCDs exhibited two absorption peaks at approximately 256 and 367 nm, corresponding to the $\pi-\pi^*$ transitions in conjugated systems and the $n-\pi^*$ transitions associated with the surface C=O and C–O functionalities[2,18]. The inset shows that the

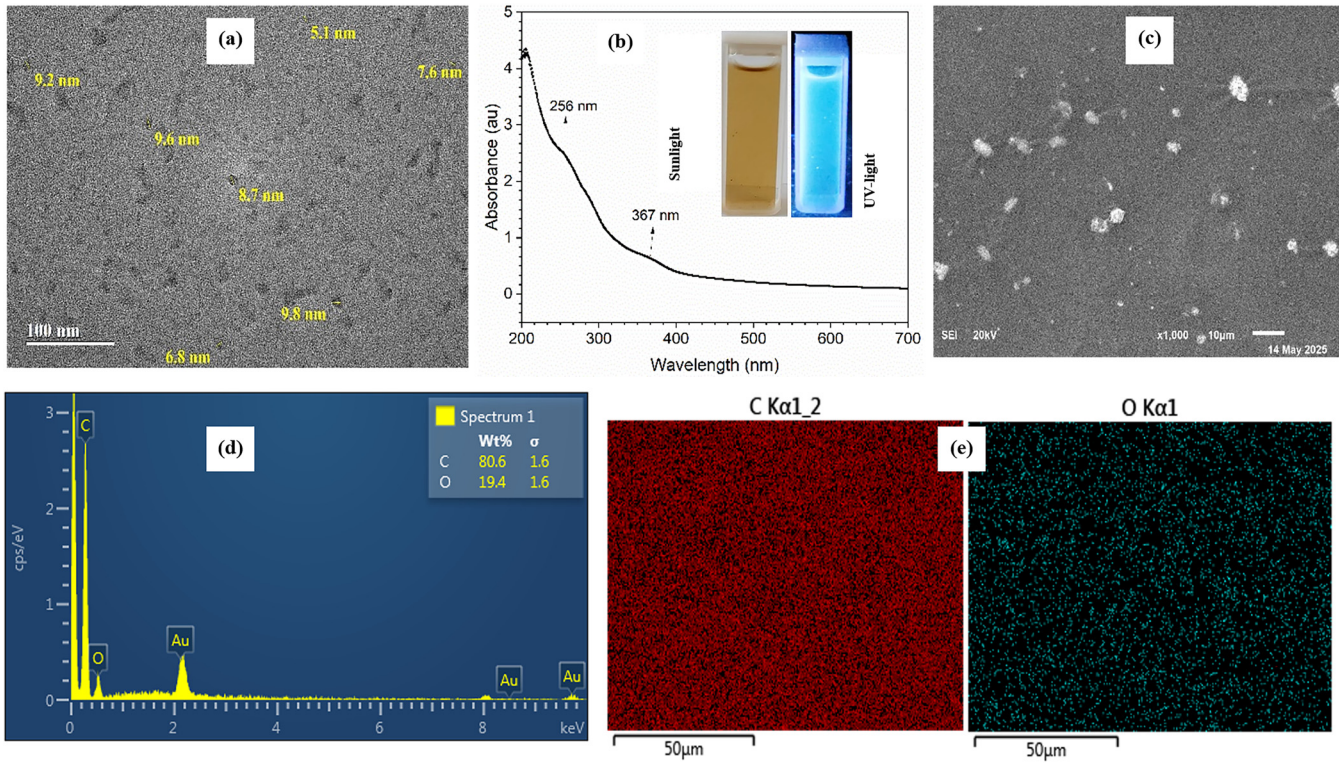

Figure 1. Results of (a) TEM, (b) UV-vis, (c) SEM, (d) EDAX and (e) elemental mapping characterizations of undoped PPCDs

PPCD solution appeared orange under visible light and emitted deep-blue fluorescence under UV light, confirming its fluorescent nature. The peaks at 1000–1275 cm^{-1} correspond to the C-H in-plane bending vibration and C–O stretching vibration, and the peaks at 1000–650 cm^{-1} correspond to the C–H out-of-plane bending vibration[13]. These results confirm that PPCDs include abundant C and O functional groups and unsaturated bonds which enhance their potential for use as corrosion inhibitors. SEM imaging and EDAX mapping (Figures 1(c–e)) further confirmed that carbon and oxygen were the primary elements in the PPCDs. Elemental analysis (Figure 1(c–e)) confirmed the absence of nitrogen in the undoped PPCDs, indicating that the observed n–π^* transitions originated solely from oxygenated groups rather than from N-containing moieties.

For N-PPCDs, TEM analysis (Figure 2a) revealed an amorphous spherical morphology similar to that observed for PPCDs, but with reduced particle sizes in the range of 2–5 nm due to nitrogen doping. The UV–vis spectrum (Figure 2b) presented a single peak at approximately 325 nm which is attributed to the n–π^* transitions involving heterocyclic structures[19,2], and the solution displayed the same orange color and blue fluorescence under UV illumination, indicating that the fluorescence properties were retained upon N doping. Figure 2(c–e) displays the results of the SEM analysis and EDAX mapping, confirming that N, C, and O are the main components of the N-PPCDs. As described above, the UV–Vis spectrum of undoped PPCDs (Figure 1b) exhibits two distinct absorption bands: a strong $\pi \rightarrow \pi$ transition near 274 nm, assigned to the aromatic C=C bonds within the conjugated carbon core, and a weaker n$\rightarrow \pi^*$ transition at approximately 367 nm corresponding to the transitions involving the C=O and C–O groups. After nitrogen doping (Figure 2b), the $\pi \rightarrow \pi^*$ transition became less distinct and merged with the n$\rightarrow \pi^*$ band to yield a single broad absorption feature centered at approximately 325 nm. This apparent disappearance of the $\pi \rightarrow \pi^*$ band is attributed to the perturbation of the π-electron system caused by nitrogen incorporation[20,6]. Nitrogen atoms introduce new electronic states (C–N, C=N, pyridinic N) within the carbon framework, disrupting the planarity and delocalization of π orbitals and enhancing charge-transfer interactions. The resulting hybridization between π and n orbitals gives rise to a blue-shifted, broadened absorption band characteristic of N-doped carbon materials. This observation confirms successful nitrogen doping and its effect on the optical and electronic properties of the CDs.

FTIR analysis of PPCDs (Figure 3(a)) revealed the presence of several functional groups; for example a broad peak at 3333 cm^{-1} can be attributed to intramolecular hydrogen bonds such as O-H[10], while the absorption peaks at 2940 and 2065 cm^{-1} can be attributed to the methyl or methylene groups[10], and the peak at 1574 cm^{-1} is attributed to the C=C vibration of the benzene ring skeleton[13]. The absorption peak at 1208 cm^{-1} corresponds to the C–O stretching vibration of carboxylic acid. The spectrum of N-PPCDs presented in Figure 3(b) reveals the presence of C=C, C–N, and C=N bonds, indicating the successful transformation of the precursors into N-PPCDs. The peak at 1597 cm^{-1} is assigned to the C−N stretching vibration[10]. The edges of the CDs are formed by chemical structures such as –CONR, which shows an absorption peak at 1651 cm^{-1}, confirming the doping process[6]. The N-PPCD shows the absorption peak of conjugated double bonds (N=C=O and C=C=N) at 2353 cm^{-1},

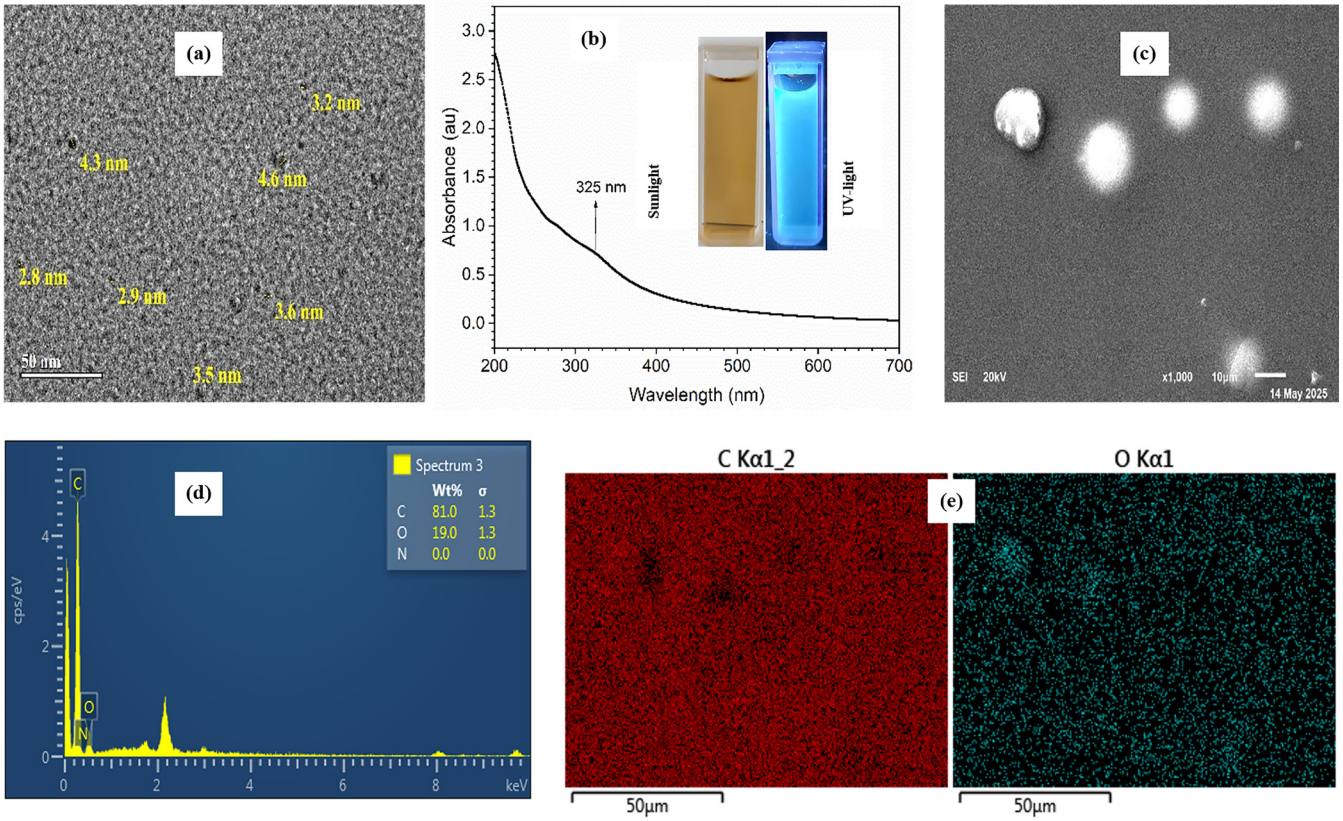

Figure 2. Results of (a) TEM, (b) UV-vis, (c) SEM, (d) EDAX and (e) elemental mapping characterizations of doped N- PPCDs

distinguishing it from its PPCD precursor[6]. The peaks centered at 1385 and 1302 cm^{-1} indicate the presence of C–N–C bonds[3]. Hence, the findings indicate that the PPCDs were successfully modified through nitrogen doping.

3.2. Corrosion Inhibition Performance.

3.2.1. Weight loss measurements. The corrosion rate and corresponding IE obtained from weight loss tests for PPCDs and N-PPCDs at two different temperatures are illustrated in Figure 4. Both the corrosion rate and IE show a clear dependence on the PPCD and N-PPCD concentrations, with increasing inhibitor concentration leading to higher IE and a corresponding decrease in the corrosion rate. This trend was attributed to the greater surface coverage of CS by the inhibitor molecules which hindered metal dissolution[21]. However, for PPCD, IE declined as the temperature was increased from 30 to 60 °C, as shown in Figure 4(a, b), likely due to the desorption of the inhibitor molecules from the CS surface and the increased molecular mobility; both of these effects reduce surface protection at elevated temperatures. The N-PPCDs showed better performance at 60 °C than at 30 °C in terms of IE. These results demonstrate the thermal stability of N-PPCDs and their ability to function at higher temperatures.

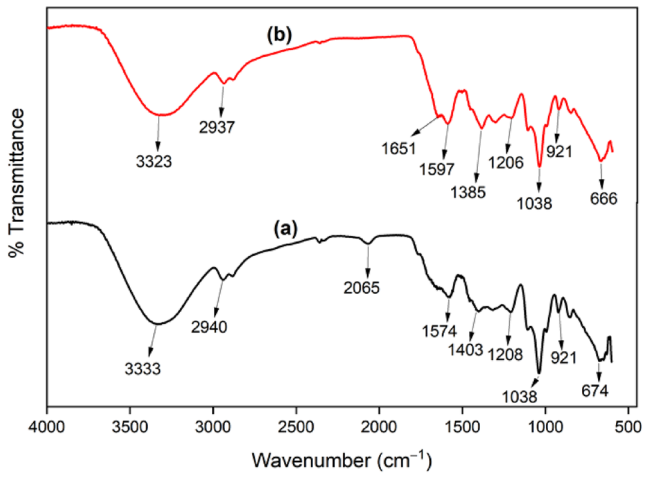

Figure 3. ATR-FTIR spectra of (a) undoped PPCDs and (b) doped N-PPCDs

3.2.2. Electrochemical measurements. PDP measurements were used to investigate the effect of the CDs on the anodic and cathodic redox reactions of CS in a 5% HCl solution. The polarization curves obtained for the CS with and without different concentrations of PPCDs and N-PPCD are shown in Figure 5. Figure 5(a-b) shows the concentration-dependent behavior of steel at a temperature of 25 °C, evaluated across the PPCD and N-PPCD concentration range of 25–200 ppm. The IE, corrosion potential (E_{corr}), corrosion current density (I_{corr}), and the anodic and cathodic slopes (β_a and β_c) were calculated by extrapolation of the anodic and cathodic current to the corrosion potentials, and the obtained results are presented in Table 1. These results indicate that the addition of CDs resulted in a noticeable decrease in both β_a and β_c accompanied by a significant reduction in the I_{corr} and E_{corr} values. These findings strongly suggest that PPCDs and N-PPCDs act as mixed-type inhibitors, effectively blocking both the cathodic and anodic reactions. The E_{corr} value

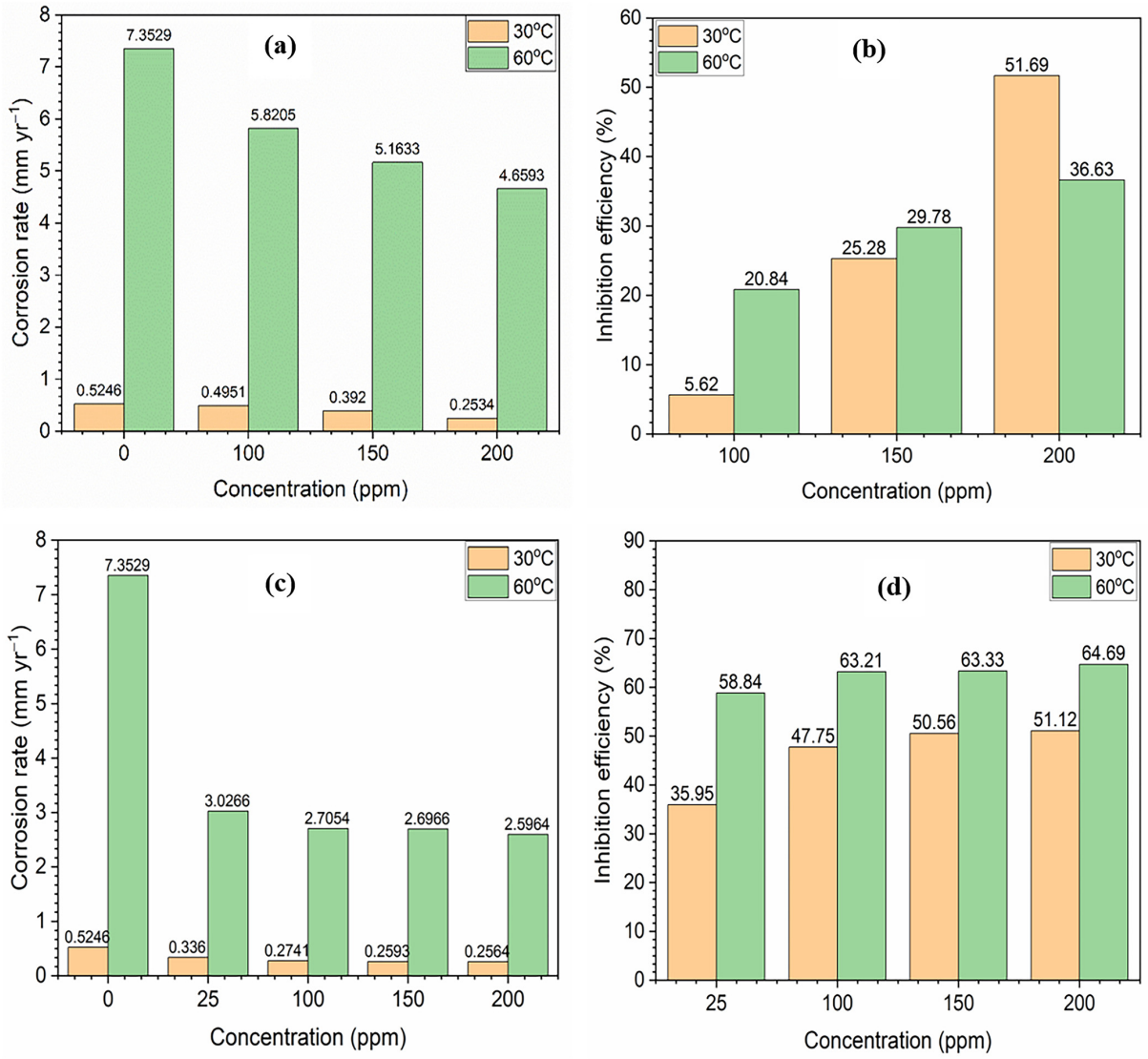

Figure 4. Corrosion rate and IE *obtained by weight loss measurements* for CS in 5% HCl solution at different concentrations of (a, b) undoped PPCDs and (c, d) doped N-PPCDs at 30 and 60 °C

became more positive after the addition of CDs, indicating that the inhibitors adsorbed onto the steel surface and blocked the active sites for corrosion.

Examination of the results presented in Table 1 shows that incorporation of PPCDs and N-PPCDs at higher concentrations increased the IE values as observed using both the PDP and LPR techniques. The highest IE values were 70.09% for PPCD and 79.58% for N-PPCD at 200 ppm obtained using the PDP technique, and 65.17% for PPCD and 75.88% for N-PPCD obtained with the LPR technique. These results showed that 200 ppm was the optimum concentration for further testing. At this concentration, the corrosion rate was 0.97 mm/y of N-PPCD, compared to 1.41 mm/y for PPCD. The higher IE and lower corrosion rate observed for N-PPCD suggested that the nitrogen-containing functional groups served as active adsorption sites, forming a protective film on the metal surface that inhibited corrosion.

The open-circuit potential (OCP) measurements at room temperature are described in the Supplementary Material, Figure S1, and section S1. The results show that the potential values shifted toward more positive potentials with increasing concentrations of PPCDs and N-PPCDs, with the most significant shift observed at 200 ppm. All inhibition curves stabilized over time, indicating the development of a protective layer on the metal surface.

To investigate the electrochemical behavior, Nyquist and Bode plots were recorded for CS in 5% HCl with varying concentrations (25–200 ppm) of PPCDs and N-PPCDs at 25 °C. Figures 6(a) and 6(c) show the Nyquist plots, and Figures 6(b) and 6(d) display the corresponding Bode plots. The Nyquist plots revealed a notable increase in the semicircle diameter upon inhibitor addition, indicating enhanced charge transfer resistance. The diameter further increased at higher inhibitor concentrations, with 200 ppm exhibiting the most significant surface coverage. N-PPCD exhibited larger diameters than PPCD at all concentrations, confirming its superior inhibition efficiency.

The Bode plots show the impedance modulus and phase angle over a frequency range between 10^5 and 10^{-2} Hz. Both PPCD

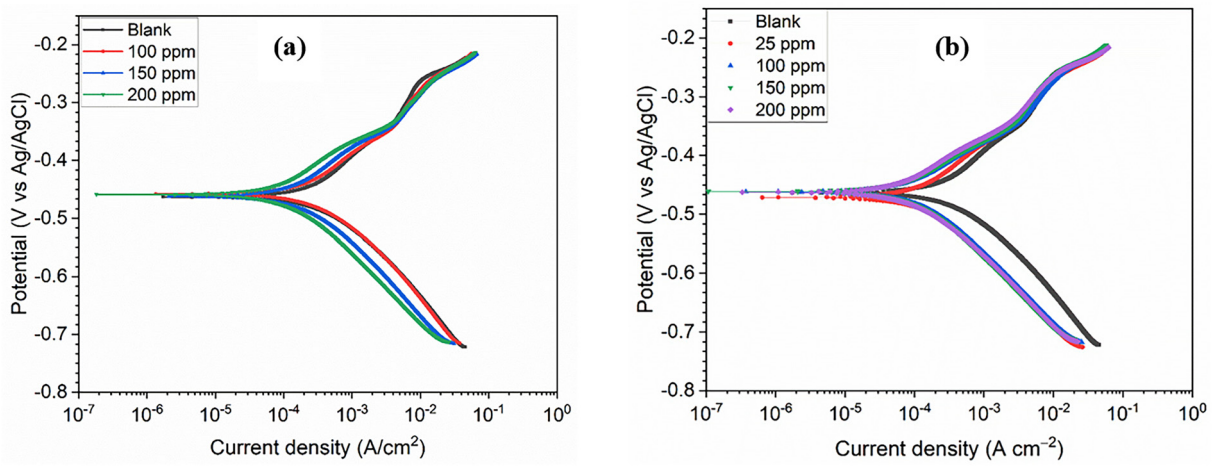

Figure 5. PDP profiles of CS immersed in 5% HCl at 25 °C, comparing the uninhibited solution with different concentrations of (a) undoped PPCDs and (b) doped N-PPCDs

and N-PPCD increased the impedance modulus, with higher values obtained with increasing concentration, suggesting effective barrier film formation on the CS surface. Additionally, the increasing peak heights in the phase angle plots with higher inhibitor concentrations indicate enhanced capacitive behavior at the metal-solution interface, which is attributed to the greater adsorption of inhibitor molecules[22].

The electrical equivalent circuit shown in the Supplementary Materials, Figure S2, and Section S2 was used to fit the experimental EIS data, and the obtained parameters are listed in Table 2. The results presented in Table 2 indicate that compared to the blank solution, the R_p values in the acidic solutions containing PPCDs and N-PPCDs increased. Specifically the R_p value increased from 51.91 Ω·cm^2 (uninhibited solution) to 151.09 Ω·cm^2 for the solution including 200 ppm PPCD, while it increased to 217.38 Ω·cm^2 for the solution with 200 ppm N-PPCD. This demonstrates that the PPCDs and N-PCDs formed a dense adsorbed layer, minimizing the number of active corrosion sites. The decrease in Y_{odl} suggests a reduced double-layer capacitance owing to the adsorbed inhibitor molecules forming a less permeable film. N-doped PPCDs consistently showed better performance than undoped PPCDs at the same concentrations, most likely due to their enhanced electron-donating capability, improved surface affinity, and denser film formation attributed to the nitrogen functional groups. At 200 ppm, the N-PPCDs provide R_{ct} and R_p of 168.3 Ω·cm^2 and 217.38 Ω·cm^2, respectively, with IE = 76.12%, outperforming undoped PPCDs. The sharp improvement in the inhibition efficiency, even at 25 ppm, of N-PPCDs emphasizes their potential as highly efficient green inhibitors at low dosages.

3.3. Surface Analysis. SEM-EDS analysis was carried out on the CS samples immersed in 5% HCl for 24 h, both with and without the addition of 100 ppm CDs, to assess surface morphology and elemental composition. The steel surface exposed to HCl without CDs exhibited significant damage owing to metal dissolution and degradation (Figure 7(a)). Exposure to HCl resulted in notable deformation and deep pits on the surface. Conversely, the micrographs of the steel surface treated with 200 ppm PPCD (Figure 7(c)) and N-PPCD (Figure 7(e)) display less surface damage with fewer imperfections compared to the untreated sample. EDS analysis of the CS sample (Figure 7(b)) revealed peaks consistent with the chemical composition of the corroded steel. In the EDS spectrum of the untreated sample, the chloride peaks indicated the adsorption of chloride ions on the steel surface, which can accelerate corrosion[10]. The reduction of the chlorine peak in the EDAX results for the PPCD-inhibited

Table 1. *PDP and LPR parameters for CS in 5% HCl without and with different concentrations of undoped PPCDs and doped N-PPCDs at 30 °C*

			PDP Technique					LPR Technique		
CDs	Conc. (ppm)	E_{corr} (mV vs Ag/AgCl)	I_{corr} (μA/cm^2)	β_a (mV/ dec)	β_c (mV/ dec)	Corrosion rate (mm/yr)	IE (%)	R_p (Ω cm^2)	Corrosion rate (mm/yr)	IE (%)
	Blank	−463.0	408.0	178.4	114.4	4.74	–	52.46	5.76	–
	100	−458.0	301.0	137.5	102.1	3.49	26.23	67.59	4.47	22.38
PPCDs	150	−462.0	199.0	137.3	105.9	2.31	51.23	102.3	2.96	48.72
	200	−459.0	122.0	120.9	106.2	1.41	70.09	150.6	2.01	65.17
	25	−472.0	156.0	125.5	112.3	1.81	61.76	145.4	2.08	63.92
N-PPCDs	100	−462.0	99.0	98.1	96.3	1.15	75.74	152.5	1.98	65.60
	150	−461.0	90.1	97.5	100.7	1.05	77.92	202.1	1.49	74.04
	200	−463.0	83.3	108.2	92.7	0.97	79.58	217.5	1.39	75.88

Table 2. *Impedance parameters for CS in 5% HCl without and with different concentrations of undoped PPCDs and N-PPCDs at 25 °C*

CDs	Conc. (ppm)	R_s (Ω cm^2)	Yo_f (mF cm^{-2} s^{n-1})	n_f	R_f (Ω cm^2)	Y_{odl} (μF cm^{-2} s^{n-1})	n_{dl}	R_{ct} (Ω cm^2)	R_p (R_f+ R_{ct}) (Ω cm^2)	$\chi^2 \times 10^{-4}$	IE (%)
	Blank	0.81	1.25	0.78	14.43	433.7	0.97	37.48	51.91	4.23	–
	100	0.84	0.51	1.0	29.45	810.9	0.78	45.72	75.17	8.76	30.94
PPCDs	150	0.65	0.23	0.99	30.11	523.7	0.79	78.74	108.85	8.54	52.31
	200	0.67	0.18	0.97	25.29	664.9	0. 79	125.8	151.09	7.41	65.64
	25	0.76	1.16	0.87	3.03	321.6	0.83	141.2	144.23	1.86	64.01
N-PPCDs	100	0.74	0.76	0.76	26.29	252.4	0.98	127.6	153.89	7.31	66.27
	150	0.76	0.87	0.76	18.29	229.3	0.92	177.9	196.19	5.84	73.54
	200	0.67	0.77	0.75	49.08	365.2	0.92	168.3	217.38	1.10	76.12

and N-PPCD-inhibited CS samples indicates that the inhibitor molecules effectively blocked the adsorption of chloride ions on the surface (Figures 7(d),(f)). Additionally, the nitrogen peak in the EDS spectrum of the N-PPCD-inhibited CS sample suggests that N-PPCD was adsorbed onto the steel surface (Figure 7(f)).

AFM surface analysis was used to examine the changes in the CS surface topography after immersion in 5% HCl solution, both with and without the inhibitor. Figure S4(a–d) show 2D and 3D micrographs of the CS submerged in the corrosive medium with and without CDs. The polished sample surface shows no visible damage (Figure S4(a)). By contrast, the sample immersed in the corrosive media exhibited clear pits and fissures, with the surface roughness increasing dramatically from 0.5166 to 68.468 nm, indicating significant corrosion. Conversely, the surface of the sample in the inhibitor-containing solution displayed minimal imperfections (Figure S4(c, d) in Supplementary Materials), with a roughness of only 2.433 nm for the PPCD-inhibited CS sample and of 1.121 nm for the N-PPCD-inhibited CS sample, which is much lower than the 68.468 nm observed for the sample without the inhibitor. These findings implied that PPCDs and N-PPCDs effectively protected steel from corrosion in harsh HCl environments. The N-doped PPCDs demonstrated superior inhibition performance, creating a more effective barrier layer that reduces metal dissolution and pitting.

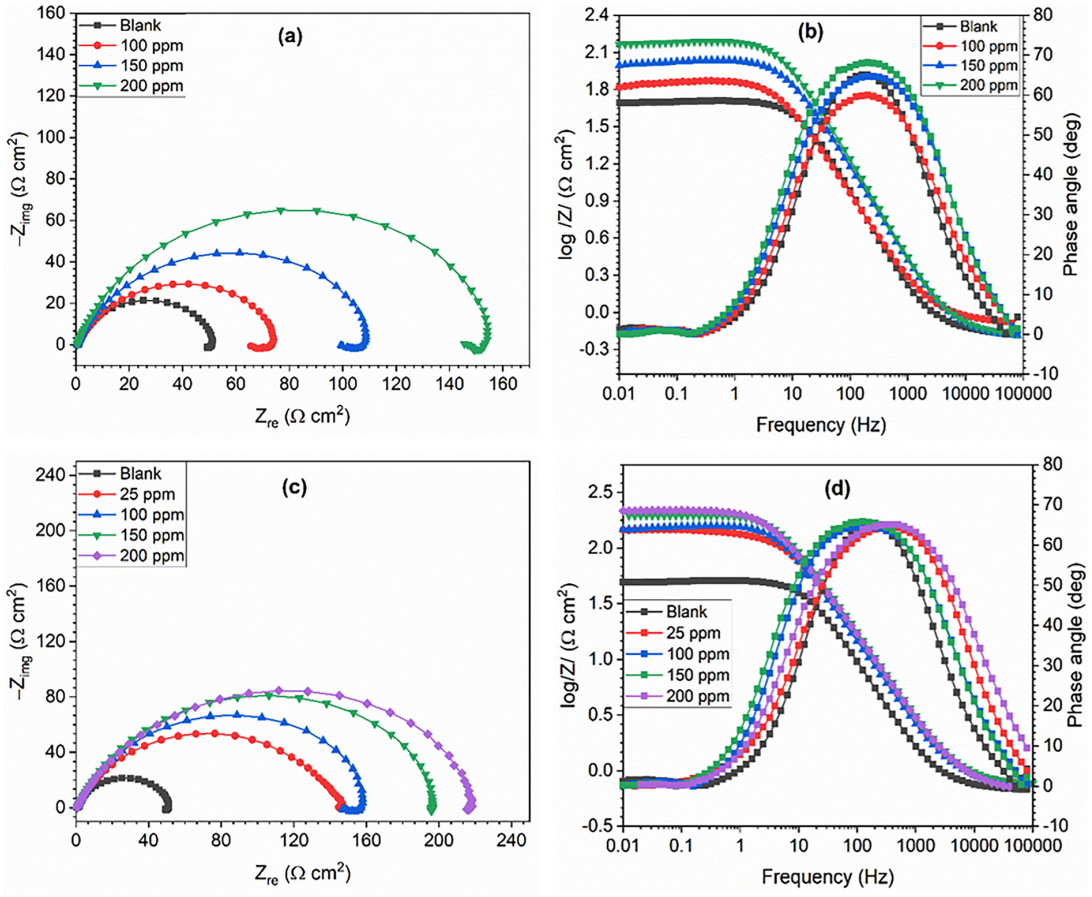

Figure 6. Impedance plots for CS in 5% HCl solution in the absence and presence of different concentrations of (a, b) undoped PPCDs and (c, d) doped N-PPCDs at 25 °C in Nyquist and Bode representations

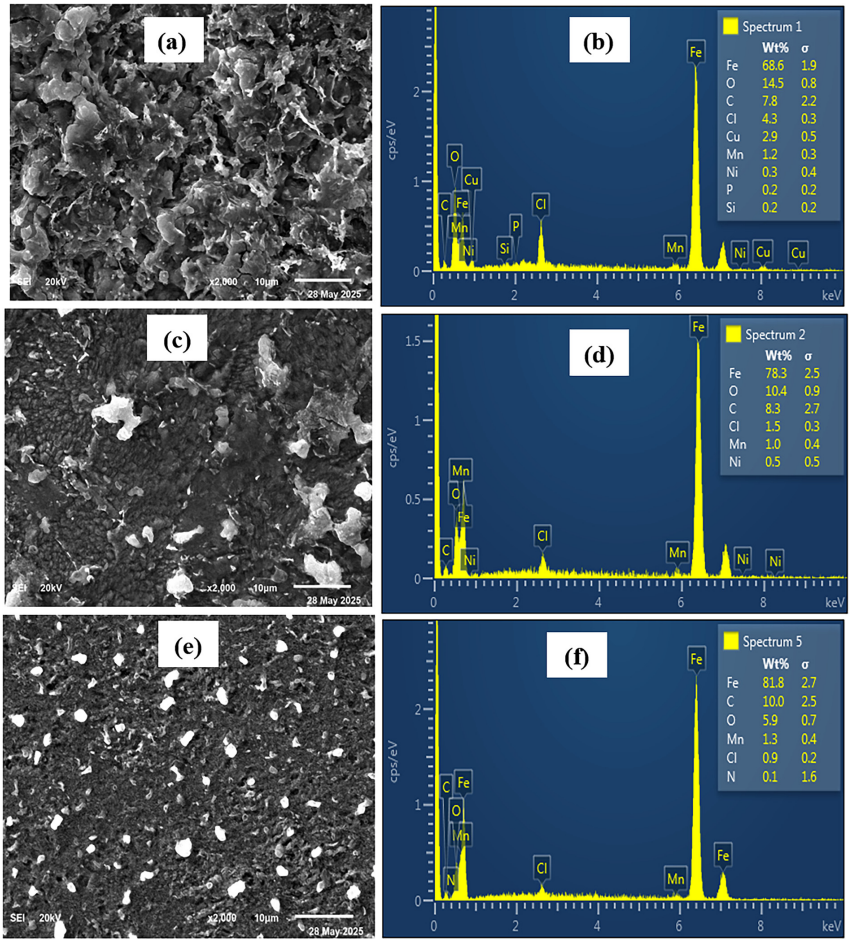

Figure 7. SEM images and corresponding EDAX spectra of CS immersed in 5% HCl (a and b) without inhibitor, (c and d) containing 100 ppm of undoped PPCDs and (e and f) containing 100 ppm of doped N-PPCDs at 30 °C after 24 h immersion

Optical profilometry was performed to further validate the microscale surface protection behavior and Figure S3 in the Supplementary Materials, Section S3 shows the 2D and 3D profilometer images obtained under identical test conditions. Table S1 summarizes the surface roughness parameters obtained from optical profilometry for CS samples exposed to 5% HCl solution, both in the absence and presence of 200 ppm of undoped PPCDs and N-doped PPCDs at 30 °C. As discussed in Section S4 of the Supplementary Materials, the sample treated with N-doped PPCDs demonstrated markedly improved surface protection. These roughness values were significantly lower than those of the blank and undoped PPCD-treated samples.

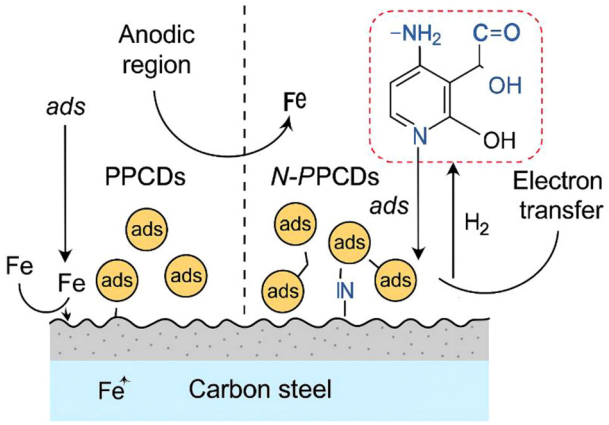

Figure 8. Proposed mechanism of corrosion inhibition of carbon steel in 5% HCl by undoped (PPCDs) and nitrogen-doped (N-PPCDs) pomegranate-peel-derived carbon dot

3.4. Possible Mechanism and Comparison to Previous Studies. Taken together, the electrochemical and surface characterization results indicate that both PPCDs and, N-PPCDs inhibit CS corrosion in 5% HCl via competitive adsorption and compact film formation at the metal/electrolyte interface with a more pronounced effect obtained for N-PPCDs. In 5% HCl, the steel surface rapidly accumulates specifically adsorbed Cl^-, while the oxygen- and nitrogen-bearing groups (carboxylates, hydroxyls; and for N-PPCDs: amines/amide/pyridinic N) on the CDs in the solution are partially protonated. The protonated functional groups in the CDs are attracted to the Cl^--decorated surface regions, displacing water and anions and binding to Fe through O-donor (PPCDs) and additional N-donor (N-PPCDs) sites via electrostatic attraction and van der Waals/π–π interactions. The adsorbed CD layer functions as a barrier to charge transfer (raising R_{ct}) and as a diffusion barrier for H^+ and Cl^-. For the cathodic reaction (H_2 evolution), the inhibitor film reduces access of H^+ to catalytic sites. For the anodic reaction ($Fe \rightarrow Fe^{2+} + 2e^-$), coverage of active Fe sites and partial

Table 3. *Comparison of corrosion inhibition performance of biomass-derived CDs for carbon steel in an acid medium*

S/N	CD inhibitor types	Metal substrate	Corrosive medium	Concentration	Inhibition efficiency (%)	Ref.
1	Acerola seed-derived CDs	Mild steel	1 M HCl	200 ppm	94.1	23
2	Pumpkin seed-derived CDs	carbon steel	1 M HCl	10 ppm	94.6	24
3	Sugarcane bagasse-derived CDs	carbon steel	1 M HCl	100 ppm	94.0	25
4	Lichi leaves derived CDs	Q235 steel	1 M HCl	200 ppm	86.1	26
5	Peanut shell-derived CDs	Cold-rolled steel	1 M HCl	50 mg/L	92.4	27
6	Grapefruit-derived CDs	Q235 steel	1 M HCl	200 ppm	94.1	13
7	*Z. bungeanum* leaves-derived CDs	Q235 steel	1 M HCl	200 ppm	95.9	28
8	Lupine seed-derived CDs	Carbon steel	1 M HCl	175 ppm	89.3	29
9	Pomegranate peel-derived CDs	Carbon steel	5% HCl	200 ppm	70.0	This study
10	N-doped-pomegranate peel-derived CDs	Carbon steel	5% HCl	200 ppm	80.0	This study

complexation of Fe^{2+} by O/N groups at the interface reduce effective dissolution. The organic layer formed by the CDs blocks both anodic dissolution and cathodic hydrogen evolution, consistent with the mixed-type behavior observed in the PDP experiments (simultaneous reductions in β_a and β_c with modest E_{corr} shifts), the increased R_p/R_{ct} and decreased double-layer admittance found by EIS measurements, and the markedly reduced roughness and suppressed chloride signals observed by AFM/SEM-EDAX. The enhanced performance of the N-PPCDs was attributed to stronger chemisorption and tighter packing due to the nitrogen functional groups, yielding a denser and less permeable film. The observed retention or improvement of IE at 60 °C for N-PPCDs suggests a chemisorption-dominated component for which the binding is less strongly affected by temperature, whereas PPCD protection shows greater decreases with higher temperature, suggesting a stronger physisorption contribution to the binding.

Hence, overall the data show (i) mixed-type inhibition (PDP: simultaneous decreases in β_a and β_c with modest, <85 mV, E_{corr} shifts), (ii) substantial increases in R_p/R_{ct} with rising inhibitor dose (EIS), (iii) marked decreases in double-layer admittance/capacitance (CPE_{dl}/Y_{odl}), and (iv) dramatically smoother surfaces with suppressed Cl signals (AFM/SEM-EDAX). This mechanism is schematically depicted in Figure 8. Together, these features support an adsorption/film formation mechanism enhanced by the nitrogen functionalities in the N-PPCDs for the inhibition of corrosion.

Table 3 compares the corrosion inhibition efficiencies of various biomass-derived CDs tested on mild or carbon steels in acidic HCl environments. The inhibition efficiencies reported in previous studies range from 86% to 96% and were typically achieved at concentrations between 10 and 200 ppm in 1 M HCl (≈3.65%). Notably, all previous studies used milder acid strengths and similar or higher doses of inhibitors. Although most reported CDs achieved 86–96% efficiency in 1 M HCl, the present study N-doped CDs exhibited 80% inhibition even in the substantially more aggressive 5% HCl medium. The 10% improvement of inhibition upon nitrogen doping confirmed the beneficial role of N-donor functionalities in enhancing chemisorption and compact film formation on the steel surface. Considering the higher acid strength and carbon steel substrate used in this study, the observed performance was comparable to or better than that of the previously reported multi-heteroatom-doped CDs, highlighting the chemical economy and green synthetic advantages of the present formulation. Additionally, the present study is the first report on the use of nitrogen-doped pomegranate peels CDs for corrosion inhibition.

4. CONCLUSIONS

This study demonstrates that CDs synthesized from pomegranate peel waste, and particularly nitrogen-doped PPCDs (N-PPCDs), can serve as effective green corrosion inhibitors of CS in acidic environments. N-PPCDs achieved superior inhibition efficiency (up to 79.58%) owing to enhanced surface interactions and film formation. Electrochemical and surface analyses confirmed the reduced corrosion rates and smoother steel surfaces in the presence of these inhibitors. Overall, N-PPCDs offer a sustainable and high-performance alternative to conventional inhibitors, supporting the use of biomass-derived nanomaterials for corrosion protection.

AFFILIATIONS AND AUTHOR DETAILS

Undergraduate Author

Ali M. Al Nasser – *Department of Materials Science and Engineering, King Fahd University of Petroleum & Minerals, Dhahran 31261, Saudi Arabia;* 0009-0008-2138-4011
Email: s202012520@kfupm.edu.sa

Authors

Hifsa Kurdshid – *Postdoctoral Fellow, Interdisciplinary Research Center for Advanced Materials, King Fahd University of Petroleum & Minerals, Dhahran 31261, Saudi Arabia;* 0000-0001-5295-1332
Email: hifsa.khurshid@kfupm.edu.sa

Corresponding Author

Saviour A. Umoren – *Research Mentor, Principal Research Scientist, Interdisciplinary Research Center for Advanced Materials, King Fahd University of Petroleum & Minerals, Dhahran 31261, Saudi Arabia.*

Department of Materials Science and Engineering, King Fahd University of Petroleum & Minerals, Dhahran 31261, Saudi Arabia; 0000-0002-8564-4897
Email: umoren@kfupm.edu.sa

ACKNOWLEDGEMENTS

The authors acknowledge the support provided by the Interdisciplinary Research Center for Advanced Materials at King Fahd University of Petroleum and Minerals.

REFERENCES

(1) He, H. J. *et al.* Exploiting machine learning for controlled synthesis of carbon dots-based corrosion inhibitors. *J. Clean. Prod.* **419**, (2023).

(2) Yang, Y., Lu, R., Chen, W., Mei, P. & Lai, L. Amphiphilic carbon dots as high-efficiency corrosion inhibitor for N80 steel in HCl solution: Performance and mechanism investigation. *Colloids Surfaces A Physicochem. Eng. Asp.* **649**, 129457 (2022).

(3) Aslam, R., Sun, X., Zhao, J., Wang, Q. & Yan, Z. Assessment of Anticorrosive Application of Biomass-Derived Carbon Quantum Dots for Mild Steel in 15% HCl Solution: Chemical and Electrochemical Studies. *Waste and Biomass Valorization* (2025) doi:10.1007/s12649-025-03090-w.

(4) Cui, M., Ren, S., Zhao, H., Wang, L. & Xue, Q. Novel nitrogen doped carbon dots for corrosion inhibition of carbon steel in 1 M HCl solution. *Appl. Surf. Sci.* **443**, 145–156 (2018).

(5) Gupta, D., Priyadarshi, R., Tammina, S. K., Rhim, J.-W. & Agrawal, G. Fruit Processing Wastes as Sustainable Sources to Produce Multifunctional Carbon Quantum Dots for Application in Active Food Packaging. *Food Bioprocess Technol.* (2024) doi:10.1007/s11947-024-03578-8.

(6) Matter, E. A., El-Naggar, G. A., Nasr, F. & Ahmed, G. H. G. Facile synthesis of N-doped carbon dots (N-CDs) for effective corrosion inhibition of mild steel in 1 M HCl solution. *J. Appl. Electrochem.* **53**, 2057–2075 (2023).

(7) Moradi, M., Molaei, R., Kousheh, S. A., T. Guimarães, J. & McClements, D. J. Carbon dots synthesized from microorganisms and food by-products: active and smart food packaging applications. *Crit. Rev. Food Sci. Nutr.* **63**, 1943–1959 (2023).

(8) Long, W. J., Li, X. Q., Zheng, S. Y. & He, C. A novel effective carbon dots-based inhibitor for carbon steel against chloride corrosion: From inhibition behavior to mechanism. *Carbon N. Y.* **218**, 118708 (2024).

(9) Ganesan, K. *et al.* Candle soot derived carbon dots as potential corrosion inhibitor for stainless steel in HCl medium. *J. Appl. Electrochem.* **54**, 89–102 (2024).

(10) Aslam, R. *et al.* Adsorption and Corrosion Inhibition Evaluation of Agro-Industrial Waste-Derived Sustainable Carbon Dots for Corrosion Protection of Q235 Steel in 5% HCl. *Langmuir* (2025) doi:10.1021/acs.langmuir.4c04571.

(11) Tengfei Xiang, Jiaqi Wang, Yanli Liang, Walid Daoudi, Wei Dong, Ruiqian Li, Xuxin Chen, Shengjun Liu, Shunli Zheng, and K. Z. Carbon Dots for Anti-Corrosion. *Adv. Funct. Mater.* **34**, 1–26 (2024).

(12) Wu, S., Wang, J., Liu, T., Guo, X. & Ma, L. Sulfosalicylic acid modified carbon dots as effective corrosion inhibitor and fluorescent corrosion indicator for carbon steel in HCl solution. *Colloids Surfaces A Physicochem. Eng. Asp.* **661**, 130951 (2023).

(13) Zheng, S. *et al.* Study on the corrosion inhibition of biomass carbon quantum dot self- aggregation on Q235 steel in hydrochloric acid. *Arab. J. Chem.* **16**, 104605 (2023).

(14) Saraswat, V. & Yadav, M. Improved corrosion resistant performance of mild steel under acid environment by novel carbon dots as green corrosion inhibitor. *Colloids Surfaces A Physicochem. Eng. Asp.* **627**, 127172 (2021).

(15) Umoren, P. S., Kavaz, D., Nzila, A., Sankaran, S. S. & Umoren, S. A. Biogenic Synthesis and Characterization of Chitosan-CuO Nanocomposite and Evaluation of Antibacterial Activity against Gram-Positive and -Negative Bacteria. *Polymers (Basel).* **14**, (2022).

(16) Xu, X. *et al.* Nitrogen-doped carbon quantum dots for effective corrosion inhibition of Q235 steel in concentrated sulphuric acid solution. *Mater. Today Commun.* **29**, 102872 (2021).

(17) Usman, B. J., Umoren, S. A. & Gasem, Z. M. Inhibition of API 5L X60 steel corrosion in CO_2-saturated 3.5% NaCl solution by tannic acid and synergistic effect of KI additive. *J. Mol. Liq.* **237**, 146–156 (2017).

(18) Zhu, M. *et al.* Insights into the newly synthesized N-doped carbon dots for Q235 steel corrosion retardation in acidizing media: A detailed multidimensional study. *J. Colloid Interface Sci.* **608**, 2039–2049 (2022).

(19) Zhu, M. *et al.* Insights into the newly synthesized N-doped carbon dots for Q235 steel corrosion retardation in acidizing media: A detailed multidimensional study. *J. Colloid Interface Sci.* **608**, 2039–2049 (2022).

(20) Xu, Z. *et al.* The n–π^* electronic transition induced by nitrogen vacancies enhances photocatalytic hydrogen production in carbon nitride. *Chem. Eng. J.* **501**, 157670 (2024).

(21) Cen, H., Chen, Z. & Guo, X. N, S co-doped carbon dots as effective corrosion inhibitor for carbon steel in CO_2-saturated 3.5% NaCl solution. *J. Taiwan Inst. Chem. Eng.* **99**, 224–238 (2019).

(22) Mourya, P., Banerjee, S. & Singh, M. M. Corrosion inhibition of mild steel in acidic solution by Tagetes erecta (Marigold flower) extract as a green inhibitor. *Corros. Sci.* **85**, 352–363 (2014).

(23) Paiva, V. M. *et al.* A new carbon quantum dot obtained from acerola (Malpighia glabra) seed waste and its application as a corrosion inhibitor of mild steel in hydrochloric acid. *Biomass and Bioenergy* **203**, 108264 (2025).

(24) Magno Paiva, V. *et al.* Pumpkin (Cucurbita maxima) seed-derived nitrogen, phosphorus, and sulfur carbon quantum dot as an inhibitor of corrosion for mild steel in HCl solution. *J. Mater. Res. Technol.* **28**, 2504–2515 (2024).

(25) Nunes, R. da S. *et al.* Sugar Cane (Saccharum officinarum L.) Waste Synthesized Si,N,S-Carbon Quantum Dots as High-Performance Corrosion Inhibitors for Mild Steel in Hydrochloric Acid. *ACS Omega* **9**, 50246–50259 (2024).

(26) Long, W.-J., Li, X.-Q., Yu, Y. & He, C. Green synthesis of biomass-derived carbon dots as an efficient corrosion inhibitor. *J. Mol. Liq.* **360**, 119522 (2022).

(27) Guan, Y., Li, X., Tan, B., Yang, S. & Deng, S. Hydrothermal synthesis of peanut shell-derived carbon dots as the novel efficient inhibitor for the corrosion of steel. *Colloids Surfaces A Physicochem. Eng. Asp.* **728**, 138517 (2026).

(28) Dong, L. *et al.* High-Efficiency Corrosion Inhibitor of Biomass-Derived High-Yield Carbon Quantum Dots for Q235 Carbon Steel in 1 M HCl Solution. *ACS Omega* **8**, 46934–46945 (2023).

(29) Abd-El-Nabey, B. A., Mahmoud, M. E., Abdelrahman, A. & Abd-El-Fatah, M. A. Effective Performance of Derived Sustainable Lupine Carbon Quantum Dots as a Superior Inhibitor Material for Carbon Steel Corrosion in a Hydrochloric Acidic Environment (1.0 Molar). *Ind. Eng. Chem. Res.* **63**, 2901–2915 (2024).